JOURNAL OF CATALYSIS **171,** 115–129 (1997)
ARTICLE NO. CA971783

The Sulfidation of γ-Alumina and Titania Supported (Cobalt)Molybdenum Oxide Catalysts Monitored by EXAFS

R. G. Leliveld,[1] A. J. van Dillen, J. W. Geus, and D. C. Koningsberger

Department of Inorganic Chemistry, Debye Institute, Utrecht University, P.O. Box 80083, 3508 TB Utrecht, The Netherlands

Received January 16, 1997; revised March 27, 1997; accepted May 30, 1997

The sulfidation of γ-alumina- and titania-supported (cobalt)molybdenum oxide catalysts has been studied with X-ray absorption spectroscopy and temperature programmed sulfidation (TPS). The catalysts were stepwise sulfided at temperatures between 298 and 673 K and their structure was determined with EXAFS spectroscopy. On alumina oxygen–sulfur exchange starts at a temperature just above room temperature resulting in the formation of monomeric and dimeric molybdenum sulfide species containing disulfide ligands. Between 448 and 523 K the disulfide ligands are reduced with hydrogen and only dimeric molybdenum sulfide species with a Mo–Mo distance of 2.77 Å remain. Above 523 K these dimers aggregate to larger MoS_2 particles. In contrast, on titania molybdenum oxide is sulfided to yield isolated molybdenum sulfide monomers at 523 K, which similarly aggregate to MoS_2 particles between 523 and 623 K. No molybdenum sulfide dimers are observed as intermediates. Both on alumina and titania all intermediates are anchored to the support via Mo–O linkages with a bond distance of 2.0 Å. The addition of Co to Mo/Al_2O_3 accelerates the rate of sulfidation, demonstrated by the TPS patterns. However, on titania a lowering of the sulfidation rate is observed next to the presence of molybdenum sulfide dimers, that are not present in the unpromoted catalyst. These observations can be ascribed to the presence of $CoMoO_4$ in the oxidic catalyst.

INTRODUCTION

Supported transition metal catalysts like those of Co, Ni, and Mo are applied in the hydrotreating of oil since the late 1920s. Many studies deal with the preparation and structure of these catalysts and the mechanism of hydrodesulfurisation (HDS), as reviewed by several authors (1–14). The active phase of these catalysts is assumed to consist of small MoS_2 platelets with Co or Ni promoter atoms decorating their edges. Originally proposed by Topsøe and coworkers (7), this so-called "CoMoS" model was confirmed by Bouwens *et al.* (15–17) and Crajé *et al.* (18, 19) by EXAFS and Mössbauer experiments. Industrially, fresh oxidic catalysts are activated by addition of compounds like CS_2 or methylsulfides to the feedstock (20). In most laboratory studies catalysts are sulfided by a mixture of H_2S and H_2. It is very likely that the conversion of the oxidic catalyst structure into the sulfided phase determines the final structure and performance of the catalyst. During the last 15 years several studies were carried out on the mechanism of sulfidation of molybdenum oxide catalysts and possible structures of intermediates.

Extensive temperature programmed sulfidation (TPS) studies of (Co promoted) molybdenum oxide on alumina were performed by Moulijn and coworkers (21–23). They concluded that sulfidation initially takes place via an O–S exchange reaction on Mo^{VI}. This exchange is followed by reduction of Mo^{VI} by means of S elimination from the formed MoO_xS_y compounds. The formed elemental sulfur reacts with hydrogen to H_2S in the temperature region from 430 to 600 K. Schrader and Cheng (24) performed a stepwise sulfidation study of Mo/Al_2O_3 and identified with *in situ* laser Raman spectroscopy the presence of molybdenum oxysulfides and reduced molybdenum oxides during sulfidation. In another Raman study Payen *et al.* (25) also reported on oxysulfides as intermediates, but with Mo reduced to Mo^{V}. Additionally, they proposed sulfido compounds and MoS_3 as transient species. EXAFS studies of Parham and Merill (26) and Chiu *et al.* (27) on sulfidation of $(Co)Mo/Al_2O_3$ reported on O–S exchange and subsequent formation and growth of MoS_2 slabs between 573 and 673 K.

In a sulfidation study of MoO_3/SiO_2 de Boer *et al.* (28) found oxysulfides only to be present at low temperature. Characterisation with EXAFS of the catalyst sulfided at 423 K showed the presence of a molybdenum sulfide species, which structure resembled that of MoS_3. The MoS_3 particles are reduced with hydrogen to MoS_2 accompanied by the evolution of H_2S as observed by Scheffer *et al.* (21). In a recent sulfidation study of uncalcined $NiMo/SiO_2$ prepared with nitrilotriacetic acid (NTA) as chelating agent Medici found no bulk MoS_3 as intermediate, but small MoS_3 like clusters with a structure probably analogous to the $[Mo_2(S_2)_6]^{2-}$ complex (29). For a complete transition from these clusters into MoS_2 the temperatures had to be raised above 583 K. XPS studies by Niemandsverdriet and coworkers on $MoO_3/SiO_2/Si(100)$ model catalysts showed the

[1] Author for correspondence. E-mail: leliveld@chem.ruu.nl.

0021-9517/97 $25.00

presence of bridging disulfide ligands during sulfidation and substantial amounts of Mo^V in an early stage of sulfidation (30, 31). These authors proposed the sulfidation mechanism to consist of an O–S exchange followed by a Mo–S redox process.

Despite all this work, there are still open questions. In a previous EXAFS study of sulfided molybdenum catalysts supported on alumina and titania we reported on the anchoring of molybdenum disulfide slabs to the support via Mo–O bonds (32). However, the results of that study were not sufficient to draw conclusions about the origin or formation of the metalsulfide-support interaction during sulfidation. Additionally, for the industrially used alumina catalysts an overview of the detailed structure of the intermediates during all stages of sulfidation is still lacking. For these reasons, the aim of this study was to retrieve detailed information about the structure of the catalyst during all stages of sulfidation and about the influence of the support. Hence, molybdenum oxide catalysts supported on alumina and titania were stepwise sulfided at temperatures between room temperature and 673 K and characterised with EXAFS. Additionally, to study the influence of the promoter, catalysts containing both Co and Mo were prepared, sulfided at various temperatures and characterised. To provide a basis for the interpretation of the EXAFS data, TPS patterns of the different catalysts were also recorded. Finally, intermediate structures present during the sulfidation of molybdenum oxide catalysts are proposed based both on our results and on available literature data.

EXPERIMENTAL

Preparation of the Catalysts

A 15 wt% MoO_3/γ-Al_2O_3 and a 4.4 wt% MoO_3/TiO_2 catalyst were prepared by incipient wetness impregnation of preshaped bodies (150–425 μm) of γ-Al_2O_3 (Ketjen CK-300, specific surface area 200 m^2/g, pore volume 0.63 ml/g) and TiO_2 (Degussa 7702, specific surface area 44 m^2/g, pore volume 0.14 ml/g, 80% anatase), respectively, with an aqueous solution of $(NH_4)_6Mo_7O_{24} \cdot 6H_2O$ (Merck, p.a.) containing 25% ammonia. The surface coverage in both catalysts was 0.70 mg Mo/m^2. $CoMo/Al_2O_3$ (3.8 wt% Co_3O_4, 14 wt% MoO_3) and $CoMo/TiO_2$ (1.1 wt% Co_3O_4, 4.3 wt% MoO_3) with an equal Co : Mo ratio were prepared by incipient wetness coimpregnation of γ-Al_2O_3 and TiO_2 with an aqueous solution containing the required amounts of $(NH_4)_6Mo_7O_{24} \cdot 6H_2O$ and $Co(NO_3)_2 \cdot 6H_2O$. All catalysts were subsequently dried with an air flow for 4 h at 298 K, dried in static air at 383 K for 16 h and calcined in air at 723 K during 16 h.

Temperature Programmed Sulfidation

Temperature-programmed sulfidation profiles were recorded in an automated microflow apparatus; 1 ml of catalyst was put on a quartz filter in an quartz lab reactor (8 mm Ø). On top of the catalyst 1 ml of quartz beads (1.5 mm Ø) was placed to ensure the gas mixture to reach oven temperature. Prior to reaction the reactor was flushed with Ar (flow rate 100 ml/min) to remove air, where after the catalyst was exposed to a 100 ml/min flow of the sulfiding mixture of $H_2S/H_2/Ar$ (10/40/50). After 30 min at room temperature the reactor temperature was linearly raised (5 K/min) to 673 K. During sulfidation the H_2S concentration of the sulfidation mixture before and after the reactor was monitored with a UV/VIS spectrophotometer (Varian, Quartz cuvets Hellma, 20 mm). The H_2S absorption was detected at $\lambda = 232$ nm.

EXAFS Data Collection

The EXAFS measurements were performed at EXAFS station 9.2 of the Wiggler beam line of the SRS at Daresbury (U.K.). The Si[220] double crystal monochromator was detuned to 50% intensity to minimise the presence of higher harmonics. The measurements were all carried out in transmission mode using optimised ion chambers as detectors. To minimise high and low frequency noise the counting time per data point varied from 1 s at $k = 3$ Å^{-1} to 3 s at $k = 20$ Å^{-1} and at least three scans were recorded and averaged. All spectra were recorded with the sample at liquid nitrogen temperature. The energy calibration of the monochromator was performed by means of a Mo-foil. The absolute value of the Mo-edge is 19,999 eV.

The catalyst samples were pressed into self-supporting wafers and mounted in an *in situ* EXAFS cell (33). The thickness of the wafer was chosen to give an absorbance (μx) of 2.5 for optimal signal to noise ratio. To prevent self-absorption for the high loaded Mo/Al_2O_3 and $CoMo/Al_2O_3$ samples the thickness of the wafer was chosen to obtain a step in absorbance of 1.0 in the edge region ($\Delta \mu x = 1$). The wafers were dried *in situ* at 393 K during 1 h in a He flow (flow rate 50 ml/min) to remove physisorbed water. The stepwise sulfidation of the catalysts was carried out in a 10% H_2S/H_2 flow during 30 min (flow rate 50 ml/min^{-1}) at temperatures ranging from 298 to 673 K (5 K/min linear heating rate). After sulfidation the samples were cooled down in H_2S/H_2 to room temperature (10 K/min) and the cell was flushed for 15 min with He to remove H_2S. The EXAFS spectrum was recorded after which the sample was allowed to reach room temperature again. Similarly the same sample was sulfided at a higher temperature in the given range and characterised with EXAFS.

EXAFS Data Analysis

Standard procedures were used to extract the EXAFS data from the measured absorption spectrum. The background was subtracted using cubic spline routines (34). Normalisation was done by dividing the data by the height of the

absorption edge at 50 eV. Phase shifts and backscattering amplitudes from reference compounds were used to calculate the EXAFS contributions: Na_2MoO_4 for the Mo–O, and MoS_2 for the Mo–S and Mo–Mo contributions. Details of the references are described elsewhere (35). Phase shifts and backscattering amplitudes of the Mo–Al and Mo–Ti contributions were theoretically calculated with the FEFF-3.1 code (36).

Multiple shell fitting of the EXAFS data was done in R-space. The difference file technique was applied, together with phase-corrected Fourier transforms to resolve the different contributions (37). Coordination numbers were corrected for the difference in absorber-backscatterer distance between the reference compound and the unknown assuming an electron mean free path of 5 Å (38).

The reliability of the calculated fit is usually expressed as the goodness of fit ε_ν^2 which includes the statistical noise on the data (39). However, it proved that the random noise of the measured data is in some cases so low that $\varepsilon_\nu^2 \gg 1$. In that case the noise is dominated by systematic errors from the measurement and data analysis. To correct the standard deviations of the structural parameters for the systematic errors, ε_ν^2 should be corrected as described by Stern *et al.* (40). Alternatively, we have chosen to express the quality of fit as the difference between the absolute or imaginary part of the Fourier transform of the experimental data with that of the model Fourier transform. These differences are described by the FT^n variance:

$$FT^n = 100\frac{\int\left(FT^n_{model}(R) - FT^n_{expt}(R)\right)^2}{\int\left(FT^n_{expt}(R)\right)^2} \qquad [1]$$

in which n represents the weight of the Fourier transform. The errors in the resulting fit parameters are estimated to be 20% in coordination number N, 1% in distance R, 10% in Debye–Waller factor $\Delta\sigma^2$ and 10% in ΔE_0.

RESULTS

Temperature Programmed Sulfidation

Figure 1 represents the normalised H_2S absorption per Mo (no corrections were made for Co) of the various catalysts versus the sulfidation temperature. Initially, just above room temperature with all catalysts a positive peak due to desorption of physisorbed H_2S was observed. At higher temperatures the catalysts started to consume H_2S, followed by a H_2S evolution peak at around 423–493 K in case of the alumina catalysts. Between 493 and 673 K the alumina catalysts showed a further uptake of H_2S. In contrast, the titania samples showed no H_2S production peak, but continuous absorption of H_2S in the range 293–673 K. Surprisingly, the normalised H_2S consumption per Mo atom is higher for the Mo catalysts in comparison with the Co promoted catalysts. Since the experimental setup was not suited for quantitative analysis no further attempts were made to study this observation. Moreover, the main purpose of the TPS experiments was to provide a basis for the interpretation of the EXAFS data in terms of the consumption and production of H_2S by the catalysts as a function of the sulfidation temperature.

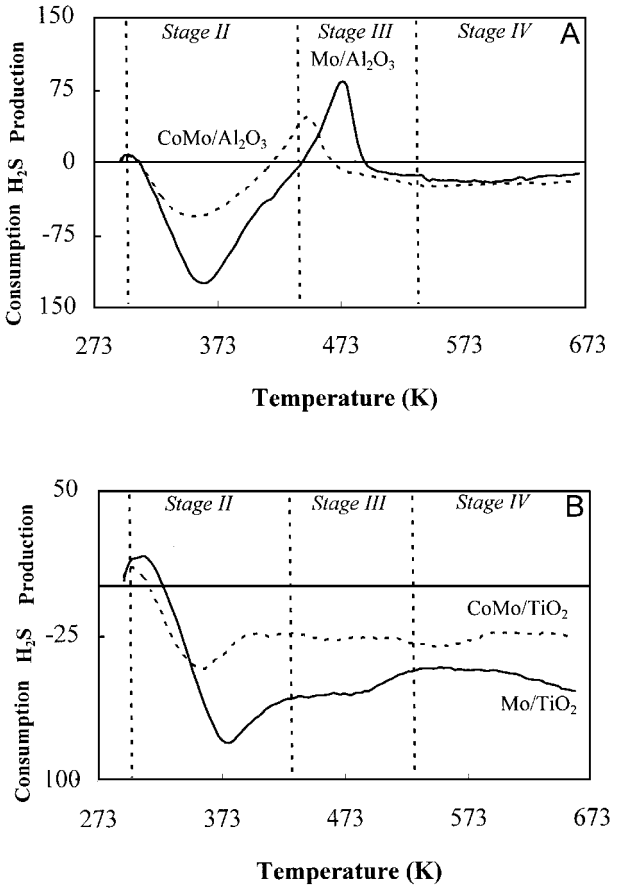

FIG. 1. TPS patterns of (A) Mo/Al_2O_3 and $CoMo/Al_2O_3$ (B) Mo/TiO_2 and $CoMo/TiO_2$.

Accordingly, the TPS pattern can roughly be divided in four temperature ranges as indicated in Fig. 1:

Stage I: sulfidation at 298 K (not shown)
Stage II: 298–448 K, uptake of H_2S
Stage III: 448–523 K, release of H_2S (for alumina catalysts)
Stage IV: 523–673 K, (renewed) consumption of H_2S.

On basis of these temperature ranges we decided to characterise the catalysts with EXAFS after sulfidation at 298 K, at every 25 K in the region 363–523 K and after sulfidation at 673 K.

In order to justify our approach of stepwise sulfidation and characterisation with EXAFS a modified sulfidation experiment was carried out. In this experiment the temperature was increased with steps of 25 K (5 K/min) and held

constant at every temperature for 30 min. It was observed that the UV-absorption dropped to the level of no H_2S consumption or production within a minute after stabilisation of the temperature. When the temperature was further raised the UV-absorption quickly returned to its former value before stabilising. These results indicated that the extent of sulfidation was solely determined by the temperature, which permitted a study of stepwise sulfidation and characterisation.

Near-Edge Region

The shape and position of the Mo–K-absorption edge contains information about the valency and local symmetry of the Mo atom. Figure 2 presents the near-edge spectra of Mo/Al_2O_3 and $(Co)Mo/TiO_2$ at different temperatures of sulfidation. The near-edge spectra of $CoMo/Al_2O_3$ were identical to those of Mo/Al_2O_3 and are therefore not shown. The spectra of both alumina and titania catalysts sulfided at room temperature contained a preedge peak that disappeared at higher temperatures. This preedge peak can be attributed to a 1*s*–4*d* bound state transition characteristic for Mo atoms in an oxidic structure. The transition probability of this formally forbidden excitation is dependent on the local symmetry around the molybdenum atom. Mixing of metal *d*-states with ligand *p*-orbitals in case of a tetrahedral or nonperfect octahedral symmetry, as encountered in molybdenum oxides, gives rise to the observed preedge feature (41, 42). The absence of this preedge peak at higher sulfidation temperatures indicated transformation of the oxidic lattice into another (sulfidic) lattice.

Additionally, the position of the absorption edge shifted to lower energy values at higher temperatures. The edge-position of the samples sulfided at room temperature agreed with an oxidation state of Mo^{VI} (MoO_3). At 673 K the edge was shifted to a lower value corresponding to the lower Mo^{IV} oxidation state (MoS_2). As Figs. 2A, B show for Mo/Al_2O_3 and Mo/TiO_2 the Mo^{IV} state was already reached at a temperature of 448 and 423 K, respectively. In contrast, $CoMo/TiO_2$ (Fig. 2C) had to be sulfided at least 498 K to completely reach a Mo^{IV} oxidation state. At intermediate temperatures the edge position for all samples was situated between that of Mo^{VI} and Mo^{IV} pointing to a mixture of Mo^{VI} and Mo^{IV} or possibly to the presence of Mo^{V}.

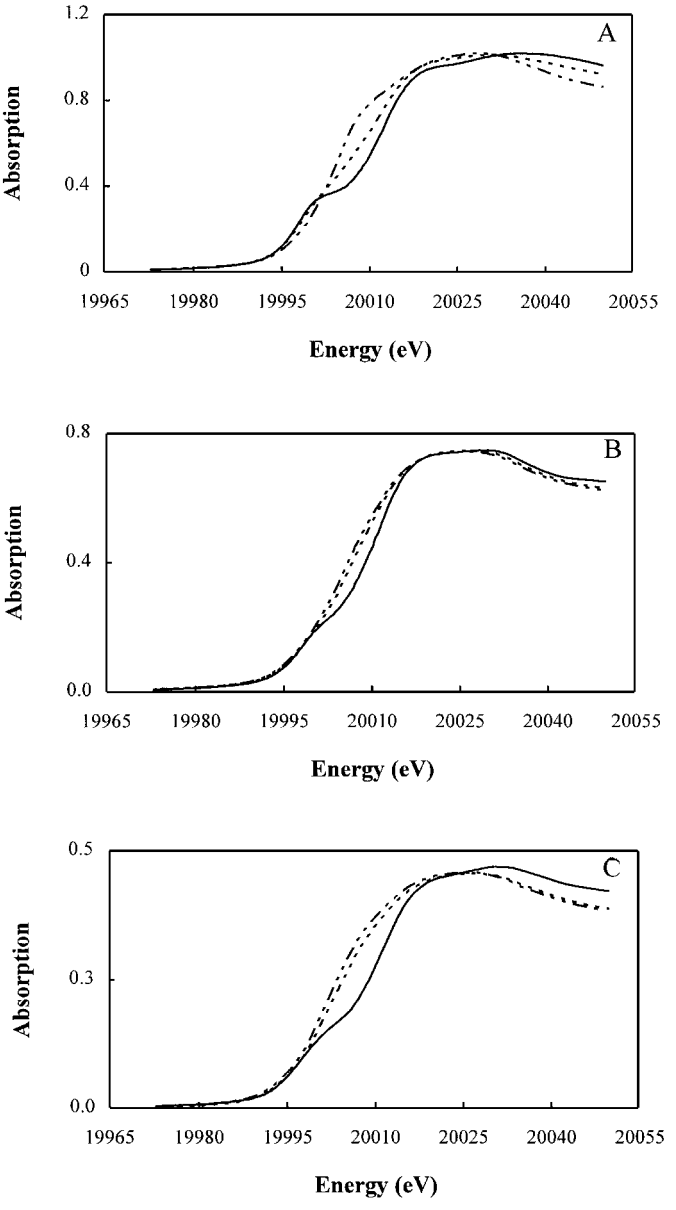

FIG. 2. XANES spectra of (A) Mo/Al_2O_3 sulfided at 298 K (———), 398 K (– – –), 448 K (— — —); (B) Mo/TiO_2 sulfided at 298 (———), 398 K (- - - - -), 423 K (— — —); and (C) $CoMo/TiO_2$ sulfided at 298 (———), 398 K (- - - - -), 498 K (— — —).

EXAFS of (Co)Mo/Al₂O₃

Eventually, after data analysis the main EXAFS results could be summarised by considering only four temperatures corresponding to or near the temperature limits of each sulfidation stage in the TPS pattern, namely 298, 423, 523, and 673 K. Figure 3 displays the experimental EXAFS data of Mo/Al_2O_3 sulfided at these four temperatures. As with the nearedge spectra the EXAFS data of $CoMo/Al_2O_3$ were identical to those of unpromoted Mo/Al_2O_3. As shown in Figs. 3A–D the data quality of the raw EXAFS data was good. The noise level was low, as expressed by a standard deviation below 0.0005 (three scans average). Based on the noise level the Fourier transform range for data analysis was chosen from 3.6 to 14.0 $Å^{-1}$. Figure 4 shows the Fourier transforms of Mo/Al_2O_3 sulfided at various temperatures together with their best fits. The fits closely matched the experimental data in the fit region between 1.0 and 3.5 Å. Below 1.0 Å the fit deviated from the measured data due to a background feature, that was difficult to subtract from the raw data.

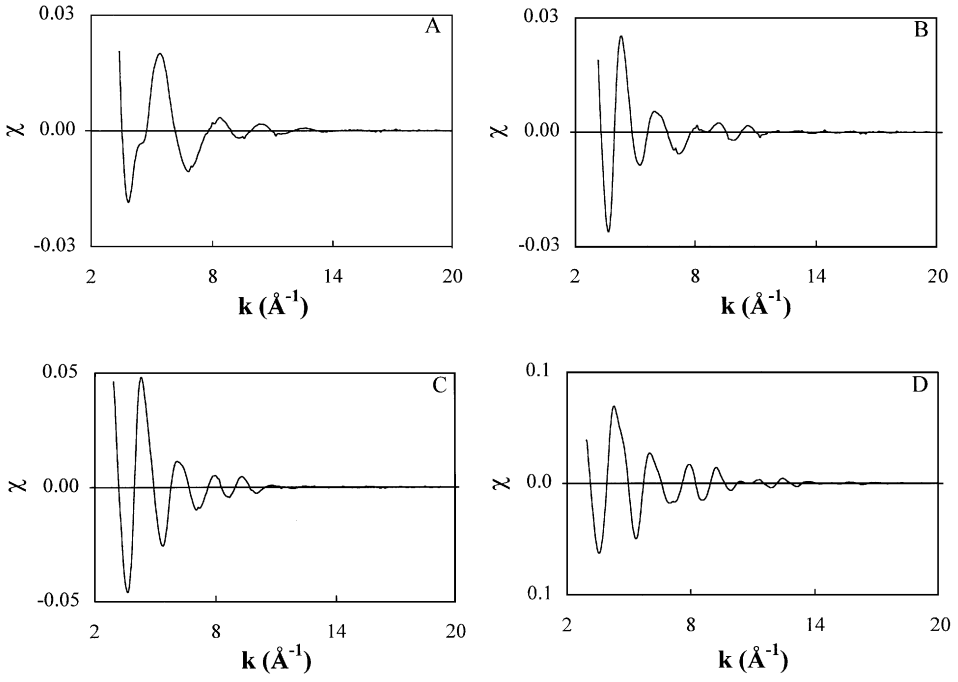

FIG. 3. EXAFS spectra (unweighted) of Mo/Al_2O_3 sulfided at (A) 298 K, (B) 423 K, (C) 523 K, (D) 673 K.

Stage I. The Fourier transform of Mo/Al_2O_3 sulfided at room temperature (Fig. 4A) mainly contained one broad peak at low R-values characteristic of Mo–O contributions (32). Comparison of the Fourier transform of the fresh oxidic catalyst and the catalyst exposed to H_2S showed no significant changes (Fig. 4A). In accordance with this, incorporation of a Mo–S contribution was not necessary to obtain a reasonable fit, confirming that at 298 K no O–S exchange had taken place. The first shell of the Fourier transform was fit by two Mo–O contributions with bond distances of 1.76 and 1.92 Å (see Table 1). Additionally, data analysis revealed the presence of Mo–Al and Mo–Mo contributions at 2.76 and 3.28 Å, respectively. A detailed description of the structure of the oxidic catalysts was already given elsewhere (32).

Stage II. Upon treatment at 363 K (Fig. 4B) the Mo/Al_2O_3 samples started to sulfide, as was indicated by a strong reduction of the amplitude of the Fourier transform around 1.3 Å and a relative increase of the amplitude of the (Mo–S) peak at around 2.0 Å. At 423 K (Fig. 4C) the amplitude around 1.3 Å reached a minimum value. This drastic decrease of the amplitude could be ascribed to destructive interference between Mo–S and Mo–O contributions (due to their phase difference of approximately π radians (43)) and to the very high Debye–Waller factor of the Mo–S contribution. Data analysis of the spectra obtained after sulfidation at 423 K showed a Mo–S coordination number of 4.3, together with a Mo–O coordination of 0.4 at 1.98 Å and a Mo–Mo coordination of 0.2 (see Table 1). The short Mo–O contribution at 1.76 Å disappeared, while the Mo–Mo bond length changed from 3.28 Å for the oxidic catalyst to 2.75 Å for the sulfided sample.

Stage III. Sulfidation at temperatures higher than 423 K led to a further increase of amplitude of the Mo–S peak at around 2.0 Å (Figs. 4D–F). This was mainly due to a

TABLE 1

Fit Parameters Mo/Alumina Supported Catalyst

Scatterer	N	$\Delta\sigma^2$ (10^{-4} Å^2)	R (Å)	ΔE_0 (eV)	Var. im.[a]	Var. ab.[b]
Stage I. *Sulfided 298 K*					3.09	0.67
O	3.4	34.0	1.76	−8.0		
O	2.8	40.0	1.92	9.0		
Al	0.4	52.9	2.76	−15.0		
Mo	0.4	60.0	3.28	8.7		
Stage II. *Sulfided 423 K*					5.14	1.35
O	0.4	−27.2	1.98	15		
S	4.3	238.6	2.46	−0.3		
Mo	0.2	−19.6	2.75	9.01		
Stage III. *Sulfided 523 K*					0.83	0.44
O	0.8	19.9	2.00	−0.8		
S	3.7	61.0	2.39	6.5		
Mo	1.0	93.1	2.78	0.3		
Mo	0.7	65.6	3.16	−4.0		
Stage IV. *Sulfided 673 K*					0.44	0.18
O	1.0	51.3	2.00	−2.0		
S	5.0	18.0	2.40	3.8		
Mo	2.9	21.0	3.15	2.4		

[a, b] Variance imaginary and absolute parts Fourier transform according to Eq. [1].

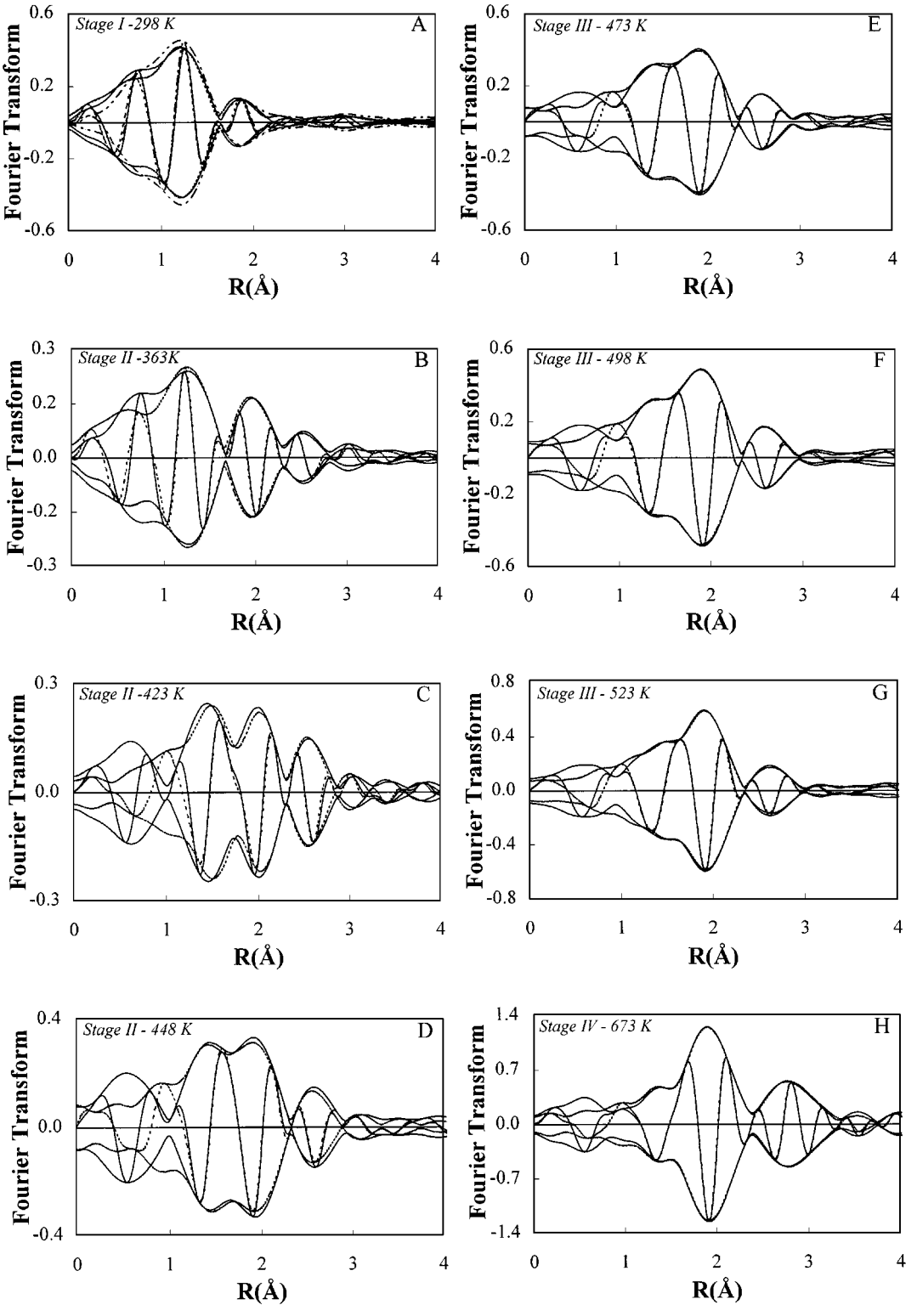

FIG. 4. Fourier transform [k^2, $\Delta k = 4.0 - 12.0$] of Mo/Al_2O_3 (———) and best fit (– – –) sulfided at (A) 298 K; oxidic catalyst (———- - - -) (B) 363 K; (C) 423 K; (D) 448 K; (E) 473 K; (F) 498 K; (G) 523 K; (H) 673 K.

lowering of the Debye–Waller factor of the Mo–S contribution, indicating that at these temperatures a less disordered structure was formed. Simultaneously, the amplitude of the peak at around 2.6 Å increased (compare Fig. 4G with 4D) due to an increasing Mo–Mo contribution. Data analysis of Mo/Al_2O_3 sulfided at 523 K (Fig. 4G) showed besides the Mo–Mo contribution at 2.77 Å a second Mo–Mo contribution with a bond distance of 3.16 Å, characteristic of MoS_2. The Mo–S coordination at this temperature had dropped to a value of 3.7. The Mo–O contribution was slightly increased from a avlue of 0.4 at 423 K to 0.8 at 523 K.

Stage IV. At temperatures higher than 523 K the Mo–Mo contribution at 2.77 Å decreased, while the 3.16 Å contribution further increased. The Fourier transforms of the alumina samples sulfided at 573 and 673 K (Fig. 4H) were characteristic of MoS_2. The Mo–S coordination had increased to a value of 5.0, while the Mo–O contribution stayed present at 2.0 Å with a coordination number of 1.0.

The values of the coordination numbers of the Mo–O, Mo–S, and Mo–Mo contributions as a function of the sulfidation temperature are presented in Fig. 5A. It is clear that both the Mo–S and Mo–Mo contribution at 2.77 Å went through a maximum value, while the Mo–O contribution had a minimum value. Additionally, the 3.16 Å Mo–Mo contribution steadily increased, starting at 523 K.

EXAFS of Mo/TiO_2

Figure 6 displays the experimental EXAFS data and Fourier transforms of Mo/TiO_2 sulfided at room temperature, 423, 523, and 673 K. The results of the data analysis are given in Table 2 and Fig. 5B. As can be seen from Fig. 5B, the general outcome of the EXAFS analyses in terms of coordination numbers was comparable to that of Mo/Al_2O_3. However, also some significant differences were found.

Stage I. The Fourier transform of Mo/TiO_2 sulfided at room temperature (Fig. 6E) was completely different from that of the fresh oxidic catalyst. An extra node was present at 1.1 Å and the maximum of the first shell was shifted to higher R-values. This different shape of the Fourier transform was due a Mo–S contribution at 2.40 Å, indicating the sulfidation of Mo/TiO_2 to start at room temperature.

Stage II. For Mo/TiO_2 sulfided at 423 K (Fig. 6F) an additional peak in the Fourier transform developed at around 3.8 Å. The analysis of this peak proved to be very difficult as will now be explained.

Figure 7A presents the Fourier transform of the raw EXAFS data minus the calculated Mo–O and Mo–S shell phase corrected for the Mo–Mo absorber–backscatterer pair. The optimum at 3.87 Å of the imaginary part of the Fourier transform implies that this contribution can be assigned to a Mo backscatterer. Alternatively, Fig. 7B shows the same Fourier transform, but now phase corrected for the Mo–Ti absorber–backscatterer pair. According to the optima in the imaginary part the contribution between

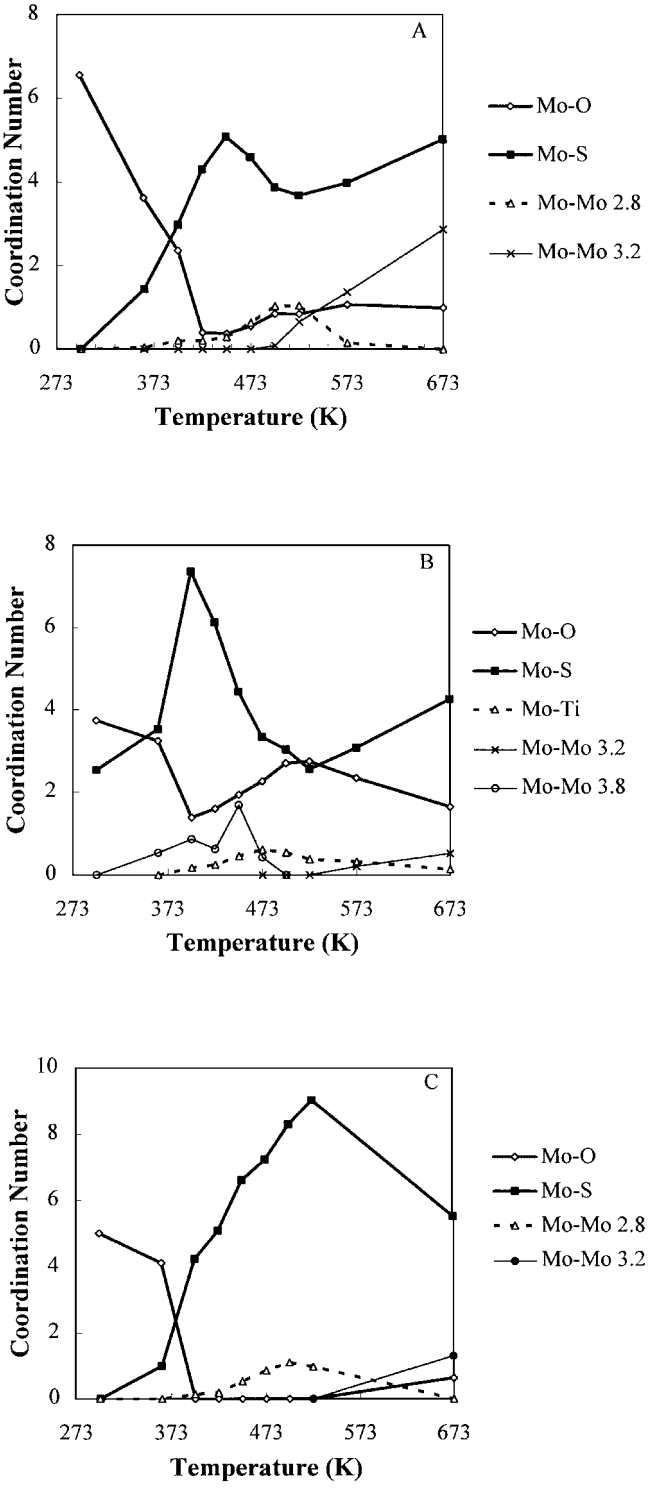

FIG. 5. Coordination numbers of the various Mo-backscatterer contributions between 298 and 673 K for (A) Mo/Al_2O_3, (B) Mo/TiO_2, and (C) $CoMo/TiO_2$.

3.5–4.5 Å can be assigned to two Mo–Ti contributions at 3.8 and 4.1 Å. However, this did not result in a converging fit.

Similarly, the peak at around 3 Å could only be fit with a Mo–Ti shell at 3.01 Å (see Fig. 7B). Assigning this

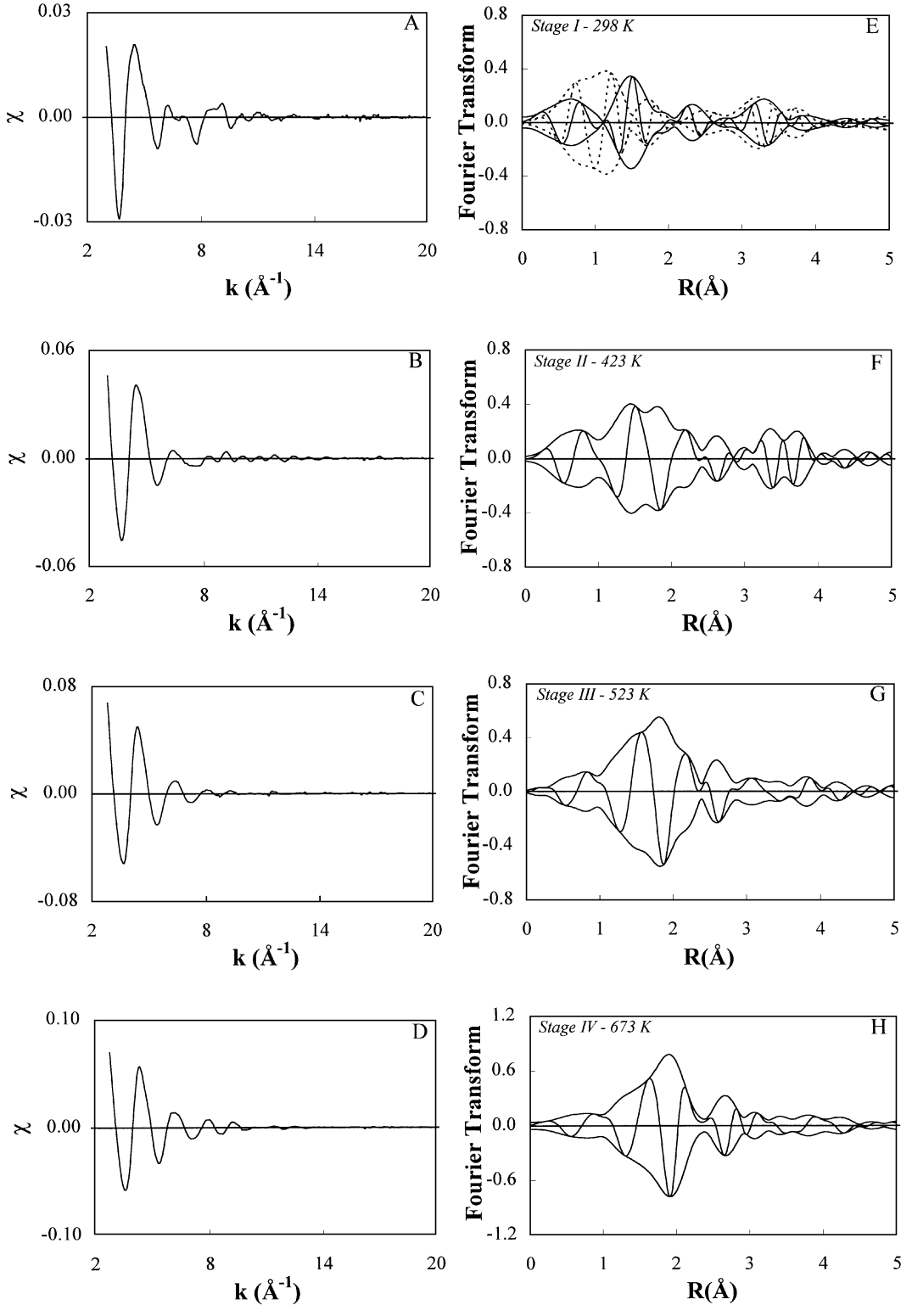

FIG. 6. EXAFS spectra (unweighted) and Fourier transforms [k^2, $\Delta k = 3.6 - 14.0$] of Mo/TiO_2 sulfided at (A/E) 298 K; oxidic catalyst (– – –); (B/F) 423 K; (C/F) 523 K; (D/H) 673 K.

TABLE 2

Fit Parameters Mo/Titania Supported Catalyst

Scatterer	N	$\Delta\sigma^2$ (10^{-4} Å^2)	R (Å)	ΔE_0 (eV)	Var. im.[a]	Var. ab.[b]
Stage I. *Sulfided 298 K*					8.32	2.82
O	0.8	79.0	1.64	15.5		
O	2.9	65.9	1.99	−2.9		
S	2.5	300.0	2.40	8.3		
Ti	0.4	46.3	2.78	10.0		
Mo	2.5	77.4	3.55	−5.3		
Stage II. *Sulfided 423 K*					2.14	0.90
O	1.6	79.9	1.95	0.9		
S	6.1	235.8	2.40	−1.1		
Ti	0.3	−23.4	2.98	1.9		
Mo	0.6	−28.2	3.87	−1.4		
Stage III. *Sulfided 523 K*					2.15	1.22
O	2.8	100.2	2.02	−0.7		
S	2.6	74.6	2.37	5.5		
Ti	0.4	−23.5	3.06	−12.1		
Stage IV. *Sulfided 673 K*					0.45	0.23
O	1.7	96.9	2.00	2.5		
S	4.3	63.5	2.39	5.9		
Mo	0.2	32.6	2.81	3.0		
Mo	1.0	32.6	3.15	3.0		
Alternative fit second shell					0.34	0.22
Ti	0.1	−53.4	2.97	−1.4		
Mo	0.5	−14.3	3.15	6.5		

[a, b] Variance imaginary and absolute parts Fourier transform according to Eq. [1].

contribution to a Mo backscatterer had to include two Mo–Mo contributions at 2.8 and 3.2 Å, which did not lead to a converging fit. The signal between 2.0 and 2.5 Å is due to an incomplete subtraction of the Mo–S contribution and was resolved after a full optimisation of all shells.

However, the high negative values for the Debye–Waller factors of the Mo–Mo and Mo–Ti contributions make the analysis results highly questionable. Moreover, regarding the results obtained with Mo/Al_2O_3 the assignment of the lower peak to a Mo–Mo contribution at around 2.8 Å and the higher peak to a Mo–Ti contribution at around 3.9 Å seems more likely. Probably, the use of a theoretical Mo–Ti reference, which assumes a Mo^0–Ti^0 pair instead of a Mo^{VI}–Ti^{IV} pair led to current outcome of the analysis. In view of the above considerations the analysis results of the second shell should be looked upon with care as indicated in Table 2.

Stage III. For Mo/TiO_2 no Mo–Mo contribution was present anymore at 523 K (Fig. 6G). Only the Mo–Ti contribution at 3.06 Å was found next to the usual Mo–O and Mo–S contributions.

Stage IV. The Fourier transform of the sample sulfided at 673 K (Fig. 6H) was characteristic of MoS_2. The second shell could be fit with a combination of Mo–Mo at 3.16 Å and Mo–Ti at 2.97 Å. However, in this case the second shell could equally be fit with two Mo–Mo contributions at 2.81 and 3.15 Å (see Table 2). The latter analysis is more realistic, since in the alternative analysis the Debye–Waller factors of the Mo–Ti and Mo–Mo contributions are again negative questioning their credibility.

EXAFS of CoMo/TiO$_2$

Figure 8 displays the raw EXAFS data and Fourier transforms of $CoMo/TiO_2$ sulfided at different temperatures. The results of the data analysis are given in Table 3 and Fig. 5C.

Stage I. $CoMo/TiO_2$ sulfided at room temperature (Fig. 8E) showed a Fourier transform that was similar to that of the fresh oxidic catalyst, although the amplitude of

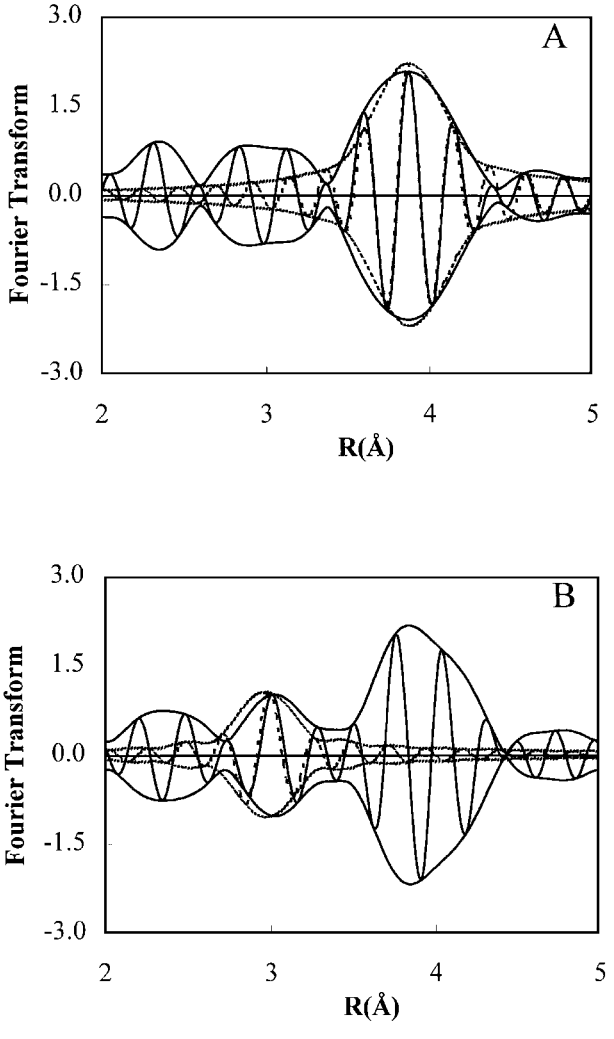

FIG. 7. Difference files for Mo/TiO_2 sulfided at 423 K (A) Mo–Mo contribution: Fourier transform (k^3, $\Delta k = 3.6 - 14.0$, Mo–Mo phase corrected) of EXAFS spectrum minus calculated Mo–S and Mo–O contributions (———) and fit with Mo–Mo contribution (– – –) (B) Mo–Ti contribution: Fourier transform (k^3, $\Delta k = 3.6 - 14.0$, Mo–Ti phase corrected) of EXAFS spectrum minus calculated Mo–S and Mo–O contributions (———) and fit with Mo–Ti contribution (– – –).

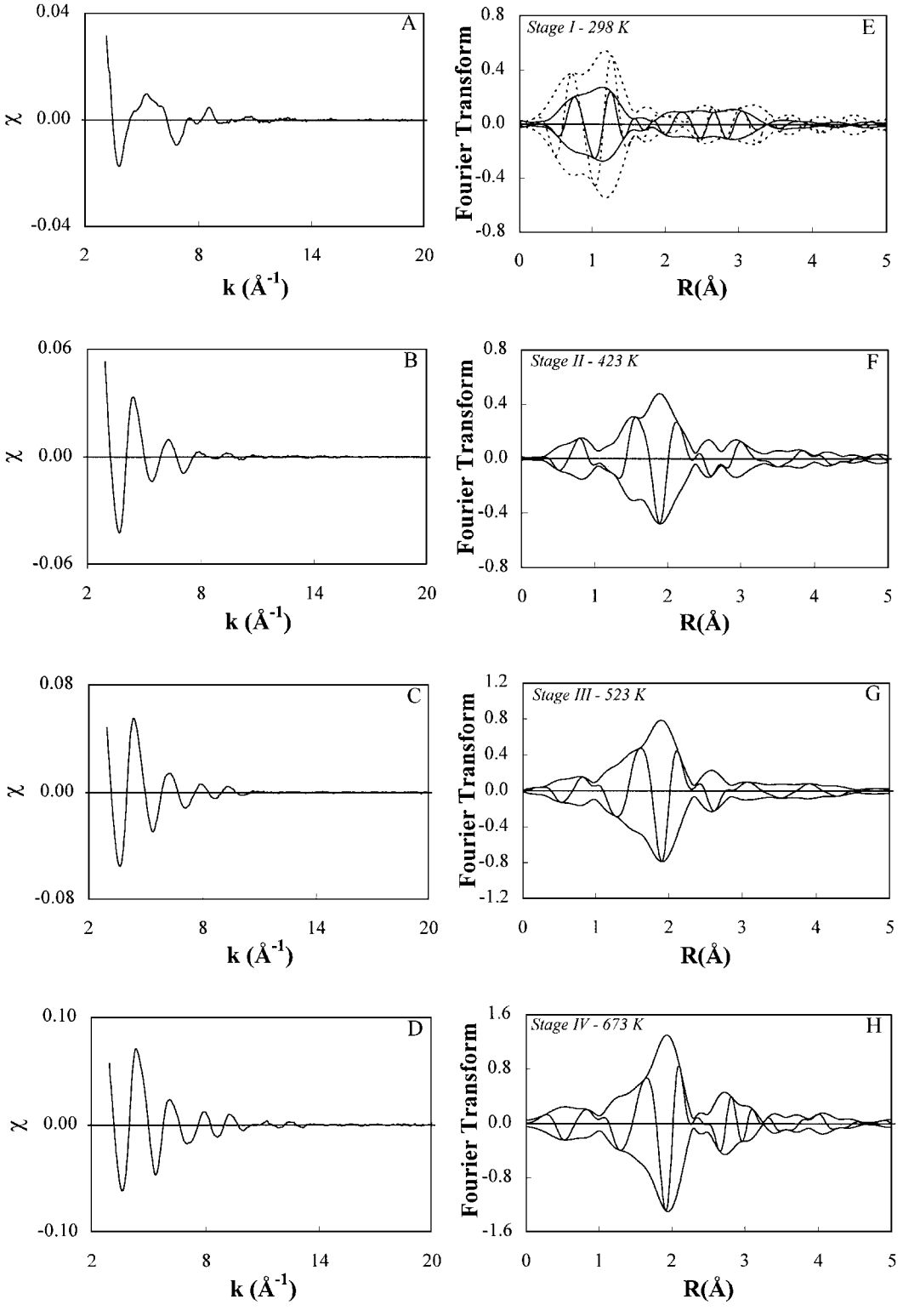

FIG. 8. EXAFS spectra (unweighted) and Fourier transforms (k^2, $\Delta k = 3.6 - 14.0$) of $CoMo/TiO_2$ sulfided at (A/E) 298 K; oxidic catalyst (– – –); (B/F) 423 K; (C/F) 523 K; (D/H) 673 K.

TABLE 3

Fit Parameters Co–Mo/Titania Supported Catalyst

Scatterer	N	$\Delta\sigma^2$ (10^{-4} Å^2)	R (Å)	ΔE_0 (eV)	Var. im.[a]	Var. ab.[b]
Stage I. *Sulfided 298 K*					4.33	1.49
O	2.5	50.2	1.75	−4.1		
O	2.5	70.1	1.94	8.6		
Ti	1.1	123.9	2.73	10.7		
Mo	1.8	100.4	3.06	−9.3		
Stage II. *Sulfided 423 K*					1.34	0.48
S	5.1	157.4	2.40	−1.1		
Mo	0.2	−1.5	2.75	3.6		
Ti	1.2	62.9	3.50	8.6		
Stage III. *Sulfided 523 K*					0.42	0.20
S	9.0	159.4	2.40	1.3		
Mo	1.0	41.6	2.73	11.8		
Stage IV. *Sulfided 673 K*					1.02	0.49
O	0.7	7.7	1.98	0.5		
S	5.5	34.9	2.40	2.8		
Mo	1.3	6.2	3.17	−1.2		

[a, b] Variance imaginary and absolute parts Fourier transform according to Eq. [1].

the first shell was much lower. However, no Mo–S contribution could be incorporated, indicating that sulfidation had not taken place at room temperature. The change in the Mo–O coordination upon sulfidation compared to the fresh oxidic catalyst is therefore hard to explain. The only difference is that the oxidic catalyst was dried at 393 K in He flow before characterisation (32), whereas the sulfided one in this study was not. The removal of physisorbed water apparently influences the structure of the molybdenum oxide entities on the titania surface.

Stages II–IV. As displayed in Fig. 5C and Figs. 8F–H the trends in the coordination numbers of the various EXAFS contributions for $CoMo/TiO_2$ were different than observed with the other samples. The maximum in the Mo–S coordination number was shifted from 398 K for Mo/TiO_2 to 523 K for the promoted catalyst. Also, the Mo–O contribution completely disappeared already at 398 K. Similar to Mo/Al_2O_3 a Mo–Mo contribution was observed at around 2.8 Å that reached a maximum value at 548 K. At 673 K only a Mo–Mo contribution at 3.16 Å was present.

DISCUSSION

The most important results can be summarised as follows:

(1) The structural parameters of the involved intermediate Mo species have been obtained as a function of the sulfidation temperature (see Fig. 5).

(2) All intermediate species during sulfidation contain Mo–O bonds with a bond length of 2.0 Å that can be ascribed to Mo–O linkages with the support as was already observed in catalysts sulfided at 673 K (32).

(3) For Mo/Al_2O_3, $CoMo/Al_2O_3$, and $CoMo/TiO_2$ intermediate species are observed during sulfidation with a Mo–Mo bond length of 2.8 Å.

(4) For Mo/Al_2O_3, $CoMo/Al_2O_3$, and Mo/TiO_2 all Mo atoms are in a +IV valency state at sulfidation temperatures of 448 and 423 K, respectively. In $CoMo/TiO_2$ all Mo atoms are in a +IV valency state after sulfidation at temperature higher than 498 K.

(5) For Mo/Al_2O_3, $CoMo/Al_2O_3$, and $CoMo/TiO_2$ sulfidation only starts at temperatures above room temperature. Sulfidation of Mo/TiO_2 already takes place at room temperature.

In the following discussion these results will be combined with available literature data to develop a model for the sulfidation of molybdenum oxide catalysts.

(Co)Mo/Al$_2$O$_3$

Stage I *(298 K)*. The EXAFS data obtained at room temperature show that the catalyst was still completely oxidic. To enable O–S exchange the temperature had to be raised above room temperature in agreement with the observed consumption of H_2S in the TPS pattern. The structure of the molybdenum oxide species can be visualised as depicted in Fig. 9 (structures A and A′). The low value of 0.4 for the Mo–Mo coordination number suggests that the main part of the Mo is present as a mononuclear species. These findings agree with the presence of predominantly MoO_4^{2-} species in the basic impregnation solution (44), which leads to a monomolybdate surface species (45).

Stage II *(298–448 K)*. The first sulfidation stage of the $(Co)Mo/Al_2O_3$ catalysts has been described by several

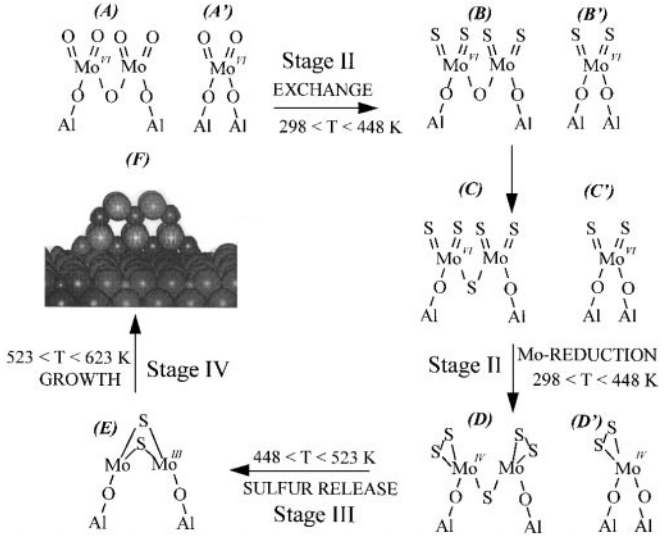

FIG. 9. Representation of the several stages of the sulfidation mechanism for Mo/Al_2O_3.

authors (21–31) as an O–S exchange on molybdenum:

$$Mo^{VI}O_y + xH_2S \rightarrow Mo^{VI}O_{y-x}S_x + xH_2O. \quad [2]$$

Weber *et al.* (46) proposed on the basis of XPS and infrared emission spectroscopy experiments that terminal Mo=O groups are more reactive towards sulfur exchange than bridging Mo–O–Mo groups.

Our EXAFS data indeed show an exchange of oxygen for sulfur. Upon sulfidation above room temperature the Mo–S coordination increases, while simultaneously the Mo–O coordination drops. The exchange can be depicted as shown in Fig. 9 (structures B and B′). Since initially the Mo–Mo distance of 3.28 Å present in the oxidic catalyst increases to 3.36 Å at 363 K it is proposed that the exchange of terminal Mo=O groups for sulfur is followed by sulfidation of (part of) the bridging Mo–O–Mo linkages. As a result dimers are formed with possible structure as structure C in Fig. 9. Monomers might react to a species like structure C′.

Weber *et al.* (46) reported that after exchange of oxygen atoms for sulfur two terminal Mo=S groups on neighbouring Mo atoms can react under formation of a bridged S_2^{2-} ligand and simultaneous reduction of Mo^{VI} to Mo^{V}. In addition Muijsers *et al.* (31) proposed that two terminal Mo=S groups on the same Mo atom can be converted to a Mo^{IV}=S_2 group. Both reactions can be represented according to:

$$Mo^{VI} + xe^- \rightarrow Mo^{(VI-x)} \quad [3a]$$

$$2S^{2-} \rightarrow S_2^{2-} + 2e^-. \quad [3b]$$

In our experiments the changing position of the Mo–K edge indicates that the O–S exchange is followed by a reduction to Mo^{V}/Mo^{IV}. At 448 K all Mo atoms are in the +IV valency state. This would suggest that a reduction to Mo^{V} under formation of bridged S_2^{2-} ligands is rare, although the Mo–Mo distance of 2.75 Å can be associated with molybdenum sulfide clusters with bridging S_2^{2-} ligands (47). However, on basis of the observed edge position it is proposed that mainly terminal S_2^{2-} ligands are formed with simultaneous reduction of the Mo^{VI} ions to Mo^{IV}. As depicted in Fig. 9 structure D and D′ then represent the type of species than are formed after sulfidation at 423/448 K. The Mo–Mo distance in the dimer is found to be 2.75 Å.

The depicted structures in Fig. 9 are not in full agreement with the structural parameters in Table 1. The Mo–S coordination is expected to be 3 instead of 4 and the Mo–O coordination should be 1. This discrepancy is described to the complexity of the Mo species that makes it difficult to obtain a good fit of the experimental EXAFS data in this temperature region. Next to destructive interference between the Mo–O and Mo–S contribution the structural disorder is very high as indicated by the high Debye–Waller factors. This does not make it impossible to obtain reasonable coordination parameters but the accuracy will be less than for more ordered structures. Accordingly, due to the overlap of the Mo–O and Mo–S shells the high disorder in the Mo–S contribution forces the calculated Mo–O coordination number to be lower. For this reason we believe that the Mo–O coordination gradually decreases from 373 to 498 K as would be expected instead of going through a minimum value as shown in Fig. 5A.

In an earlier study on Mo/SiO_2 catalysts the presence of a MoS_3 as an intermediate during sulfidation was assumed to be present (28). Although the structure of MoS_3 is still a matter of debate and is described both as a linear chain (48, 49) and as an aggregation of triangular Mo_3-sulfur clusters (50) both models invoke a Mo–Mo distance of about 2.77 Å and the presence of bridging disulfide ligands. The low value of 0.2 for the Mo–Mo coordination number suggests that at 423 K the majority of the Mo atoms is present as a mononuclear species (e.g., species D′ in Fig. 9), which makes the presence of MoS_3 or a MoS_3 like species as intermediate highly unlikely.

Stage III *(448–523 K)*. The next stage in the sulfidation mechanism has to account for both the observed H_2S release in the TPS and the decrease of the Mo–S coordination number as determined with EXAFS.

Muijsers *et al.* (31) reported that in complexes containing both terminal and bridging S_2^{2-} ligands the terminal S_2^{2-} groups can undergo reductive elimination to elemental sulfur, while simultaneously the bridging S_2^{2-} groups are reduced to S^{2-} ligands. Weber *et al.* (51) suggested that in the sulfidation of MoO_3 a bridging S_2^{2-} group can be reduced by hydrogen to a terminal S^{2-} ligand and H_2S. However, since under the conditions of high temperature and the presence of H_2 terminal S^{2-} ligands are not stable, their formation here is not very likely.

We propose that in this stage a kind of reductive elimination of the terminal S_2^{2-} groups takes place followed by reaction with H_2 leading to formation of reduced Mo centers and H_2S. (Transformation of D(D′) into E in Fig. 9). Although only the genesis of bridging S^{2-} ligands is depicted the formation of bridged S_2^{2-} groups (and Mo^{II} centers) might also take place. The occurrence of these types of reactions has been described by Diemann *et al.* (51). The creation of Mo^{II} sites through reductive elimination of sulfur from corner and edge sites in MoS_2 was reported by Müller *et al.* (52) in their study on the adsorption of carbon monoxide on reduced MoS_2/alumina catalysts. The value of 1.0 for the Mo–Mo contribution at 2.78 Å suggests that the mononuclear Mo species have formed dimers or even larger aggregates. The appearance of a Mo–Mo contribution at 3.16 Å, characteristic of MoS_2, indicates that also larger particles are formed. The remaining presence of the Mo–O contribution indicates that the Mo species are still stablised by the support, which prevents the sintering of the coordinatively unsaturated Mo species.

It is likely that on cooling to room temperature under H_2S/H_2 chemisorption of H_2S takes place on the coordinatively unsaturated Mo atoms explaining the higher Mo–S coordination number found with EXAFS. Since the position of the preedge still corresponds to a Mo^{IV} oxidation state also oxidation of the reduced Mo centers has to take place during cooling down, likely accompanied by formation of S_2^{2-} ligands.

Stage IV *(523–673 K).* After the release of sulfur the TPS pattern displays a further uptake of H_2S. At the same time, according to the EXAFS analysis, the Mo–Mo contribution at 2.77 Å quickly decreases, while the Mo–Mo contribution at 3.16 Å, characteristic of MoS_2, further increases. Clearly, the Mo-dimers sinter to larger clusters with the MoS_2 structure (structure F) as is shown in Fig. 9. Since the Mo–O coordination remains nearly constant at a value of about 1 the Mo atoms clearly stay in close contact with the support. In fact one would expect a decrease of the Mo–O contribution, since sintering occurs through sulfidation of Mo–O–Al linkages. Likely, the changes of the Mo–O coordination number occur within the limits of accuracy, which are influenced by the high degree of structural disorder and the interference between the Mo–O and Mo–S contribution as mentioned above.

Mo/TiO_2

The sulfidation of titania-supported Mo samples proceeds differently than those of alumina. Figure 5B shows that the sulfidation of Mo/TiO_2 already starts at room temperature. This can be explained by the presence of larger molybdenum oxide particles on titania compared to alumina (N_{Mo-Mo} of 2.5 and 0.4, respectively), which are more susceptible to sulfidation. When the temperature is raised the MoO_xS_y particles disintegrate indicated by the decrease of the Mo–Mo coordination number from a value of 2.5 at 298 K to 0.6 at 423 K. Simultaneously, the exchange of lattice oxygen for sulfur causes the Mo–Mo distance to increase from 3.55 to 3.87 Å. Finally, at 523 K no Mo backscatterer contribution is present in the Fourier transform, pointing to the formation of mononuclear or highly distorted MoO_xS_y species. The increase of the Mo–Ti contribution is in accordance with such a disintegration of MoO_xS_y particles. Based on the EXAFS data (despite the drawbacks concerning the credibility of the Mo–Ti contribution as explained in the results section) the structure of the MoO_xS_y clusters at 523 K can be described as mononuclear Mo species linked to two support oxygens and two terminal sulfur atoms.

Similar to alumina the Mo–S coordination number goes through a maximum value with increasing temperature. It is assumed that between 398 and 523 K an identical reduction of S_2^{2-} ligands takes place. However, the absence of the expected H_2S release peak in the TPS profile, as observed for alumina, seems in contradiction with this assumption. However, this might well be ascribed to the nature of the titania support. Huisman (53) showed that surface oxygen ions of titania can be exchanged by sulfur to a considerable degree. Thus the sulfur liberated from the MoO_xS_y clusters reacts with the support according to:

$$TiO_2 + xH_2S \rightarrow TiO_{2-x}S_x + xH_2O. \quad [4]$$

When the temperature is raised from 523 to 673 K the molybdenum sulfide monomers aggregate to MoS_2, as can be seen from the Mo–Mo contribution at 3.16 Å. In accordance, the Mo–Ti contribution drops to a lower value. It was already pointed out that at 673 K this Mo–Ti contribution can be equally well fit with a Mo–Mo contribution at 2.80 Å. This distance is close to the Mo–Mo distance of 2.77 Å found for the dimer species in alumina.

Influence of the Addition of Co

The addition of Co to Mo/Al_2O_3 catalyst causes no observable change in the EXAFS data. However, the TPS profiles (see Fig. 1) are clearly different. The shift of the H_2S release peak to lower temperatures on addition of Co agree with the results of Moulijn and coworkers (54). These authors concluded that Co accelerates the sulfiding of Mo, which is, however, not observed in the EXAFS data. This discrepancy is hard to explain and might have to do with the different character of a TPS and EXAFS experiment. TPS experiments are dynamic experiments in which the temperature is continuously raised, while in EXAFS experiments the system is allowed to equilibrate at definite temperatures of sulfidation. If Co accelerates the rate of sulfidation, but not the extent of sulfidation, this is not observed with EXAFS. Furthermore, the H_2S/H_2 ratio used in the EXAFS experiments is different from the TPS experiments. Alternatively, one might argue that the sulfiding of cobalt oxide species is superimposed on the TPS pattern of the molybdenum oxide species, causing a shift of the maximum of the H_2S release peak to lower temperatures.

Yet, it is difficult to study the effect of the presence of a promoter on the rate of sulfiding as Co also influences the initial dispersion of the molybdenum oxide species. It was shown that on alumina the addition of Co (both coimpregnation and sequential impregnation) leads to an increase of the particle size of the molybdenum oxide species (32). It is expected that larger particles are more liable to sulfidation offering another explanation for the observed shift in the TPS pattern.

In contrast, the addition of Co to Mo/TiO_2 significantly lowers the sulfidation rate of Mo as is clear from Fig. 5C and the TPS profile (Fig. 1). The lower sulfidation rate might be related to smaller molybdenum oxide particles in the promoted catalyst. Smaller particles are better stabilised by the titania surface and less susceptible to sulfidation. However, the particle size for both samples is not very different (N_{Mo-Mo} of 2.5 versus 1.8) and also the rapid decline of the

Mo–O contribution at 398 K for the promoted sample does not support this explanation. A possible explanation is formation of $CoMoO_4$ on titania. From the former discussion for Mo/TiO_2 it became clear that the interaction between molybdenum oxide or its precursor and the titania surface is rather poor. This will favour the interaction of Mo with Co leading to $CoMoO_4$. $CoMoO_4$ is indeed known to sulfide at higher temperatures than MoO_3 (55), in agreement with our results. The very high values for the Mo–S coordination number (up to 9 at 523 K) and the absence of the Mo–O contribution are due to high structural disorder as discussed above for Mo/Al_2O_3.

Regarding the structure of the catalyst at 523 K the presence of a Mo backscatterer at 2.73 Å in $CoMo/TiO_2$ points to a dimer structure with bridging disulfide ligands like structure (B) in Fig. 9. Sulfidation at 673 K changes this structure directly into MoS_2 by reduction of the disulfide ligands. The absence of a H_2S release peak is due to sulfidation of the titania surface as for Mo/TiO_2.

Influence of the Metal Oxide-Support Interaction

Analysis of the EXAFS data shows anchoring of Mo clusters to the support via Mo–O–X (X = Al or Ti) bondings with a Mo–O distance of 2.0 Å, as reported earlier (32). The current results indicate that these Mo–O–X linkages originate from the oxidic catalysts and partly remain throughout all stages of the sulfidation process.

Comparing the sulfidation of molybdenum supported on silica (28, 29), alumina, and titania reveals the influence of the support and particle size of the precursor on the intermediates. On silica the metal oxide support interaction is weak, resulting in rather large MoO_3 particles after calcination. These particles readily sulfide at low temperature to form most probably a MoS_3 bulk-like intermediate. The MoS_2 particles formed in reduction of MoS_3 are not bonded to the support and therefore are rather large ($N_{Mo-Mo} = 4.7$) (28). When bonded with the NTA complex the "Mo" particles are smaller resulting in monomers and dimers as intermediates with MoS_3 features (29). The MoS_2 particles after sulfidation at 673 K are small ($N_{Mo-Mo} = 3.0$).

On alumina molybdenum oxide particles are well dispersed and more difficult to sulfide since they are bonded to the support. As shown in this study, throughout the sulfidation process intermediate MoO_xS_y monomers and dimers remain in strong interaction with surface oxygen atoms and formed MoS_2 slabs are also fairly small ($N_{Mo-Mo} = 2.9$). On titania the initial dispersion of molybdenum oxide is less than on alumina which increases susceptibility to sulfidation. However, the better match between the titania surface structure and supported molybdenum sulfide clusters induces formation of only Mo-sulfide monomers. The ultimate dispersion of the MoS_2 slabs is very high and a description as small molybdenum sulfide clusters rather than as MoS_2 ($N_{Mo-Mo} = 0.5$) is appropriate.

In conclusion a combination of initial dispersion of molybdenum oxide particles, predominantly controlled by the kind of support and the precursor, and the "match" between the surface of the support and formed intermediates both determine the structure of intermediates and the final MoS_2 dispersion.

CONCLUSIONS

This study showed that the support influences the sulfidation of molybdenum oxide supported catalysts with respect to structural intermediates formed and the final dispersion of the MoS_2 slabs. A combination of initial dispersion of molybdenum oxide particles, influenced by the support and mode of preparation, and the "match" between the surface of the support and intermediates both determine the particle sizes of the molybdenum sulfide intermediates and the final MoS_2 slabs.

This study enabled us to describe the structure of the intermediates during sulfidation. Both on alumina and titania all intermediates are anchored to the support via Mo–O bondings of 2.0 Å. Initially, alumina oxysulfides are formed that are readily reduced to molybdenum sulfide monomers and dimers containing disulfide ligands. Above 448 K the disulfide ligands are reduced with hydrogen to yield molybdenum sulfide dimers with a Mo–Mo distance of 2.77 Å. Above 523 K these dimers aggregate to MoS_2 particles. Titania molybdenum oxide particles are sulfided to yield molybdenum sulfide monomers at 523 K, which also aggregate to MoS_2 at higher sulfidation temperatures.

The addition of Co to Mo/alumina has no effect on the kind of intermediates formed during sulfidation. However, the rate of the sulfidation as indicated by the TPS profile is increased. On titania the promotion of Mo with Co has a pronounced effect. The rate of sulfidation is considerably lower, due to the formation of $CoMoO_4$ during preparation, that is less susceptible to sulfidation.

ACKNOWLEDGMENTS

Barbara Mojet and Gert van Dorssen are acknowledged for their assistance at the SRS in Daresbury. Akzo-Nobel Research Center Amsterdam is gratefully acknowledged for the financial support.

REFERENCES

1. Massoth, F. E., *Adv. Catal.* **27**, 265 (1978).
2. Gates, B. C., Katzer, J. R., and Schuit, G. C. A., "Chemistry of Catalytic Processes." McGraw-Hill, New York, 1979.
3. Ratnasamy, P., and Sivasanker, S., *Catal. Rev.-Sci. Eng.* **22**, 401 (1980).
4. Grange, P., *Catal. Rev.-Sci. Eng.* **21**, 135 (1980).
5. Keely, W. M., Jerus, P., Dienes, E. K., and Hausberger, A. L., *Catal. Rev.-Sci. Eng.* **26**, 485 (1984).
6. Dellanay, F., *Appl. Catal.* **16**, 135 (1985).
7. Topsøe, H., Clausen, B. S., Topsøe, N. Y., and Pedersen, E., *Ind. Eng. Chem. Fund.* **25**, 25 (1986).

8. Topsøe, H., Clausen, B. S., *Appl. Catal.* **25**, 273 (1986).
9. Prins, R., de Beer, V. H. J., and Somorjai, G. A., *Catal. Rev.-Sci. Eng.* **31**, 1 (1989).
10. Luck, F., *Bull. Soc. Chim. Belg.* **100**, 781 (1991).
11. Breysse, M., Portefaix, J. L., and Vrinat, M., *Catal. Today* **10**, 489 (1991).
12. Delmon, B., *Catal. Lett.* **22**, 1 (1993).
13. Chianelli, R. R., Daage, M., and Ledoux, M. J., *Adv. Catal.* **40**, 177 (1994).
14. Startsev, A. N., *Catal. Rev.-Sci. Eng.* **37**, 353 (1995).
15. Bouwens, S. M. A. M., Prins, R., de Beer, V. H. J., and Koningsberger, D. C., *J. Phys. Chem*. **94**, 3711 (1990).
16. Bouwens, S. M. A. M., van Veen, J. A. R., Koningsberger, D. C., de Beer, V. H. J., and Prins, R., *J. Phys. Chem*. **95**, 123 (1991).
17. Bouwens, S. M. A. M., van Zon, F. B. M., van Dijk, M. P., van der Kraan, A. M., de Beer, V. H. J., van Veen, J. A. R., and Koningsberger, D. C., *J. Phys. Chem*. **146**, 375 (1994).
18. Crajé, M. W. J., de Beer, V. H. J., and van der Kraan, A. M., *Bull. Soc. Chim. Belg.* **100**, 953 (1991).
19. Crajé, M. W. J., de Beer, V. H. J., and van der Kraan, A. M., *Appl. Catal.* **70**, L7 (1991).
20. Hallie, H., *Oil Gas J.* **80**, 69 (1982).
21. Scheffer, B., de Jonge, J. C. M., Arnoldy, P., and Moulijn, J. A., *Bull. Soc. Chim. Belg.* **93**, 751 (1984).
22. Arnoldy, P., van den Heijkant, J. A. M., de Bok, G. D., and Moulijn, J. A., *J. Catal.* **92**, 35 (1985).
23. Mangus, P. J., Poels, E. K., and Moulijn, J. A., *Ind. Eng. Chem. Res.* **32**, 1818 (1993).
24. Schrader, G. L., and Cheng, C. P., *J. Catal.* **80**, 369 (1983).
25. Payen, E., Kasztelan, S., Houssenbay, S., Szymanski, R., and Grimblot, J., *J. Phys. Chem*. **93**, 6501 (1989).
26. Parham, T. G., and Merill, R. P., *J. Catal.* **85**, 295 (1984).
27. Chiu, N-S., Bauer, S. H., and Johnson, M. F. L., *J. Catal.* **98**, 32 (1986).
28. de Boer, M., van Dillen, A. J., Koningsberger, D. C., and Geus, J. W., *J. Phys. Chem*. **98**, 7862 (1994).
29. Medici, L., and Prins, R., *J. Catal.* **163**, 38 (1996).
30. de Jong, A. M., Borg, H. J., van Ijzerdoorn, L. J., Soudant, V. G. F. M., de Beer, V. H. J., van Veen, J. A. R., and Niemandsverdriet, J. W., *J. Phys. Chem*. **97**, 6477 (1993).
31. Muijsers, J. C., Weber, Th., van Hardeveld, R. M., Zandbergen, H. W., and Niemandsverdriet, J. W., *J. Catal.* **157**, 698 (1995).
32. Leliveld, R. G., Van Dillen, A. J., Geus, J. W., and Koningsberger, D. C., *J. Catal.* **165**, 184 (1997).
33. Vaarkamp, M., Mojet, B. L., Kappers, M. J., Miller, J. T., and Koningsberger, D. C., *J. Phys. Chem*. **99**, 16067 (1995).
34. Van Zon, J. B. A. D., Koningsberger, D. C., Van Blik, H. F. J., and Sayers, D. E., *J. Chem. Phys.* **82**, 5742 (1985).
35. Bouwens, S. M. A. M., Prins, R., de Beer, V. H. J., and Koningsberger, D. C., *J. Phys. Chem*. **94**, 3711 (1990).
36. Mustre de Leon, J., Rehr, J. J., and Zabinsky, S. I., *Phys. Rev. B* **44**, 4146 (1991).
37. Duivenoorden, F. B. M., Koningsberger, D. C., Uh, Y. S., and Gates, B. C., *J. Am. Chem. Soc.* **108**, 6524 (1986).
38. Kampers, F. W. H., Engelen, C. W. R., Van Hooff, J. H. C., and Koningsberger, D. C., *J. Phys. Chem*. **94**, 8574 (1990).
39. Lytle, F. W., Sayers, D. E., and Stern, E. A., *Physica B* **158**, 701 (1988).
40. Stern, E., Newville, M., Ravel, B., Yacoby, Y., and Haskel, D., *Physica B* **208/209**, 117 (1995).
41. Kutzler, F. W., Natoli, C. R., Misemer, D. K., Doniach, S., and Hodgson, K. O., *J. Phys. Chem*. **73**, 3274 (1980).
42. Mensch, C. T. J., van Veen, J. A. R., van Wingerden, B., and van Dijk, M. P., *J. Phys. Chem*. **92**, 4961 (1988).
43. Teo, B-K., and Lee, P. A., *J. Am. Chem. Soc.* **101**, 2815 (1979).
44. Baes, C. F., and Mesmer, R. E., "The Hydrolysis of Cation," Wiley, New York, 1976.
45. van Veen, J. A. R., Hendriks, P. A. J. M., Romers, E. J. G. M., and Andrea, R. R., *J. Phys. Chem*. **94**, 5275 (1990).
46. Weber, Th., Muijsers, J. C., van Wolput, J. H. M. C., Verhagen, C. P. J., and Niemandsverdriet, J. W., *J. Phys. Chem*. **100**, 14144 (1996).
47. Cohen, S. A., and Stiefel, E. I., *Organomet.* **4**, 1689 (1985).
48. Chien, F. Z., Moss, S. C., Liang, K. S., and Chianelli, R. R., *Phys. Rev. B* **29**, 4606 (1984).
49. Hibble, S. J., Rice, D. A., Pickup, D. M., and Beer, M. P., *Inorg. Chem*. **34**, 5109 (1995).
50. Weber, Th., Muijsers, J. C., and Niemandsverdriet, J. W., *J. Phys. Chem*. **99**, 9194 (1995).
51. Diemann, E., Weber, Th., and Müller, A., *J. Catal.* **148**, 288 (1994).
52. Müller, B., van Langeveld, A. D., Moulijn, J. A., and Knözinger, H., *J. Phys. Chem*. **97**, 9028 (1993).
53. Huisman, H. M., Ph.D. thesis, University of Utrecht, 1994.
54. Scheffer, B., de Jonge, J. C. M., Arnoldy, P., and Moulijn, J. A., *Bull. Soc. Chim. Belg.* **93**, 751 (1984).
55. de Boer, M., Ph.D. thesis, Utrecht University, 1992.